

# Semiparametric Copula Estimation for Spatially Correlated Multivariate Mixed Outcomes: Analyzing Visual Sightings of Fin Whales from Line Transect Survey

Tomotaka Momozaki<sup>1</sup>, Tomoyuki Nakagawa<sup>2,5</sup>, Shonosuke Sugasawa<sup>3</sup>  
and Hiroko Kato Solvang<sup>4</sup>

<sup>1</sup>Department of Information Sciences, Tokyo University of Science

<sup>2</sup>School of Data Science, Meisei University

<sup>3</sup>Faculty of Economics, Keio University

<sup>4</sup>Marine Mammals Research Group, Institute of Marine Research

<sup>5</sup>Statistical Mathematics Unit, RIKEN Center for Brain Science

## Abstract

For marine biologists, ascertaining the dependence structures between marine species and marine environments, such as sea surface temperature and ocean depth, is imperative for defining ecosystem functioning and providing insights into the dynamics of marine ecosystems. However, obtained data include not only continuous but also discrete data, such as binaries and counts (referred to as mixed outcomes), as well as spatial correlations, both of which make conventional multivariate analysis tools impractical. To solve this issue, we propose semiparametric Bayesian inference and develop an efficient algorithm for computing the posterior of the dependence structure based on the rank likelihood under a latent multivariate spatial Gaussian process using the Markov chain Monte Carlo method. To alleviate the computational intractability caused by the Gaussian process, we also provide a scalable implementation that leverages the nearest-neighbor Gaussian process. Extensive numerical experiments reveal that the proposed method reliably infers the dependence structures of spatially correlated mixed outcomes. Finally, we apply the

proposed method to a dataset collected during an international synoptic krill survey in the Scotia Sea of the Antarctic Peninsula to infer the dependence structure between fin whales (*Balaenoptera physalus*), krill biomass, and relevant oceanographic data.

**Key words:** Dependence modeling; Extended rank likelihood; Quasi-posterior; Gaussian process; Markov chain Monte Carlo

## 1 Introduction

Many marine ecosystems are characterized by several levels of interactions between marine species such as populations of fish, birds, and sea mammals, and the marine environment (Mann and Lazier, 2005). Understanding the nature of these interactions is imperative because they define ecosystem functioning and provide insights into the effects of climate change on the dynamics of marine ecosystems (Tett et al., 2013). The data used to investigate these interactions are usually obtained through scientific surveys, and the outcomes of abiotic and biotic observations are mixed with continuous (e.g., acoustic registration, biomass, abundance) and discrete numbers (e.g., counted and sighted data). In addition, the data are spatially correlated. Therefore, it is difficult to estimate the interactions between marine species and environmental factors in marine ecosystems accurately using these data.

To model the interactions among variables, multivariate analysis is an ubiquitous tools, with many methodologies developed, such as factor analysis, principal component analysis (e.g., Manly and Alberto, 2016), graphical modeling (e.g., Jordan, 2004), and copulas (e.g., Joe, 2014). In particular, copulas are attractive tools for explicitly modeling dependence structures without modeling marginal distributions and can also be successfully applied even when outcomes are mixed (i.e., outcomes include both continuous and discrete variables). As techniques for estimating copulas, Hoff (2007) proposed the extended rank likelihood for parametric copulas and developed a simple Gibbs sampler for Bayesian inference on copulas. Although these methods are useful for modeling the dependence structure, multivariate observations are assumed to be independent of each other. However, beginning with the example of marine ecosystems mentioned above, in many applications such

as epidemiology, climatology, medicine, and sociology, multivariate data with location information are often available, and spatial correlation must be appropriately considered; otherwise, the estimation of the dependence structure among outcomes could be severely biased.

To demonstrate the potential effects of spatial correlation in dependence modeling, we consider simulated multivariate data with 300 samples and four mixed outcomes, the detailed settings of which are explained in Section 4. Figure 1 shows the estimation results of the method in Hoff (2007) (denoted as BGC) when applied to the simulated data. The 95% credible intervals of the BGC do not include most of the true values, indicating that the inference of the dependence structure is severely biased without considering the spatial correlation. However, the 95% credible intervals based on the proposed method (spBGC) presented in Section 3 can suitably capture the true correlation. Therefore, for multivariate data equipped with location information, it is essential to adequately consider the spatial correlation to make a correct inference on the dependence structure.

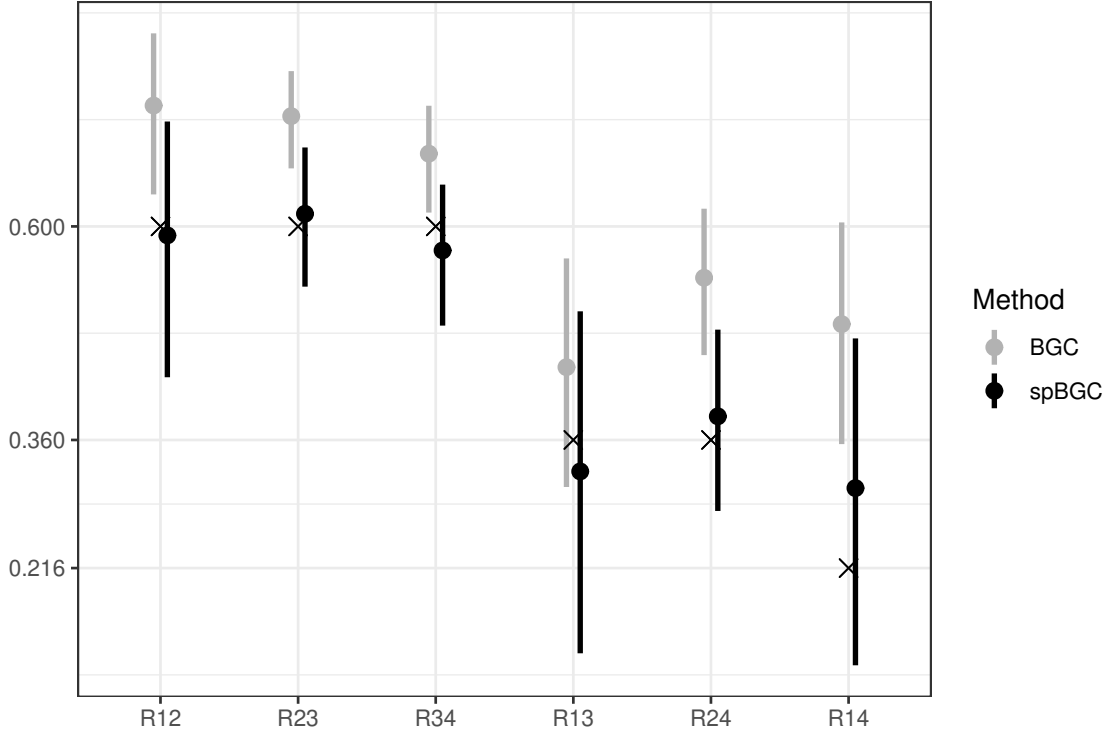


**Figure 1:** The 95% credible interval and the posterior median of each correlation coefficient by Hoff (2007)’s (BGC) and our proposed methods (spBGC): Cross marks denote true values.

Our proposal defines a spatially correlated hierarchical model combined with extended

rank likelihood. By doing so, we can provide a semiparametric copula inference that considers the spatial correlation between multivariate observations. To this end, we consider a spatial hierarchical model that embeds a Gaussian copula for the dependence among mixed outcomes and a Gaussian process for spatial correlation. We refer to it as a *spatial Gaussian copula*. For Bayesian inference, we develop an efficient algorithm to calculate the posterior of the dependence structure based on the extended rank likelihood using the Markov chain Monte Carlo (MCMC) method. Because the Gaussian process is computationally intractable for large datasets, for example, in terms of matrix operation cost and memory (Heaton et al., 2019; Liu et al., 2020), we scale our algorithm using the nearest-neighbor Gaussian process (Datta et al., 2016). Extensive numerical experiments reveal that our proposed procedure successfully accounts for the spatial correlation and correctly infers the dependence structure among outcomes. Remarkably, as the spatial correlation among observations becomes stronger, our proposed method outperforms Hoff (2007)’s, which does not consider spatial correlation.

Related work in spatial modeling includes several studies on modeling multivariate spatial data. For example, Dey et al. (2022) and Krock et al. (2023) proposed efficient modeling (relatively high-dimensional) of multivariate spatial data for Gaussian outcomes, whereas Feng and Dean (2012) and Torabi (2014) considered multivariate models based on generalized linear mixed models. Furthermore, attempts have been made to use copulas in multivariate spatial modeling, such as Musafer et al. (2017), Krupskii et al. (2018), Krupskii and Genton (2019), and Gong and Huser (2022). Because the above methods consider the joint estimation of both marginal and dependence structures, one may lose the efficiency of the estimation by a large number of nuisance parameters in the marginal distributions, while the estimation of the dependence could be biased owing to potential specifications of the marginal distributions. Hence, it is more reasonable to model the dependence structure directly, as in the proposed method.

The remainder of this paper is organized as follows. Section 2 introduces the extended rank likelihood and semiparametric Bayesian inference for the dependence structure proposed by Hoff (2007). Section 3 proposes a semiparametric Bayesian inference for the dependence structure in spatially correlated mixed outcomes and develops an efficient algorithm for computing the posterior using the MCMC. The algorithm is then extended

to a more scalable implementation using the nearest-neighbor Gaussian process, even for large spatial datasets. Section 4 presents the simulation results, including a comparison with the method of Hoff (2007), to validate the usefulness of the proposed method. Section 5 presents the application of the proposed method using real data collected during an international synoptic krill survey in the Scotia Sea of the Antarctic Peninsula. Section 6 provides directions for future research. The R code for implementing the proposed method is available in the GitHub repository (<https://github.com/t-momozaki/spBGC>).

## 2 Extended rank likelihood for semiparametric copula estimation

Suppose that we observe  $p$ -dimensional observations of mixed outcomes  $\mathbf{y}_i = (y_{i1}, \dots, y_{ip})^\top$  for  $i = 1, 2, \dots, n$ , where each variable could be a variety of outcomes, such as continuous, count, and ordered variables. Here, we are interested in the dependence structure of  $p$  outcomes. The marginal distributions of each component in  $\mathbf{y}_i$  are not of interest and are the nuisance parameters in Hoff (2007) and our framework. Let  $\mathbf{z}_i$  be a  $p$ -dimensional continuous latent variable for  $\mathbf{y}_i$ . Then, we consider the following Gaussian copula model:

$$\begin{aligned} \mathbf{z} = (\mathbf{z}_1^\top, \mathbf{z}_2^\top, \dots, \mathbf{z}_n^\top)^\top &\sim N_{pn}(\mathbf{0}, \mathbf{I}_n \otimes \mathbf{R}), \\ y_{ij} &= F_j^{-1}[\Phi(z_{ij})], \end{aligned} \tag{1}$$

where  $\mathbf{R}$  is the  $p \times p$  correlation matrix and  $\mathbf{I}_n$ ,  $\otimes$ ,  $F_j^{-1}$ , and  $\Phi(\cdot)$  denote the  $n \times n$  identity matrix, Kronecker product, inverse of an unknown univariate cumulative distribution function, and cumulative distribution function of the standard normal distribution, respectively. Here, we focus on correlation matrix  $\mathbf{R}$  as the dependence structure. In this model, Hoff (2007) defines the following extended rank likelihood:

$$L(\mathbf{R}) = \Pr(\mathbf{z} \in D | \mathbf{R}) = \int_D \phi_{pn}(\mathbf{z}; \mathbf{0}, \mathbf{I}_n \otimes \mathbf{R}) d\mathbf{z}, \tag{2}$$

where  $\phi_k(\mathbf{x}; \boldsymbol{\mu}, \boldsymbol{\Sigma})$  is the  $k$ -dimensional multivariate normal density with a mean vector  $\boldsymbol{\mu}$  and a variance-covariance matrix  $\boldsymbol{\Sigma}$ . Observing  $\mathbf{y} = (\mathbf{y}_1^\top, \mathbf{y}_2^\top, \dots, \mathbf{y}_n^\top)^\top$  indicates that  $\mathbf{z}$  must lie within the set

$$D = \{\mathbf{z} \in \mathbb{R}^{pn} : \max(z_{kj} : y_{kj} < y_{ij}) < z_{ij} < \min(z_{kj} : y_{ij} < y_{kj})\}$$

as  $F_j$  is a nondecreasing function and observing  $y_{ij} < y_{i'j}$  for any  $i \neq i'$  implies that  $z_{ij} < z_{i'j}$ . Note that this likelihood depends only on the parameter of interest,  $\mathbf{R}$ , and not on the nuisance parameters,  $\mathbf{F} = (F_1, F_2, \dots, F_p)^\top$ . It can be regarded as a type of marginal likelihood in the presence of nuisance parameters and can be derived in terms of the decomposition theorem on sufficient statistics. That is,

$$\begin{aligned} p(\mathbf{y}|\mathbf{R}, \mathbf{F}) &= p(\mathbf{z} \in D, \mathbf{y}|\mathbf{R}, \mathbf{R}) \\ &= \Pr(\mathbf{z} \in D|\mathbf{R})p(\mathbf{y}|\mathbf{z} \in D, \mathbf{R}, \mathbf{F}) \end{aligned}$$

and to estimate  $\mathbf{R}$ , it is sufficient to use only  $\Pr(\mathbf{z} \in D|\mathbf{R})$ . Function (2) is called the extended rank likelihood because it is derived from the marginal probability of the ranks, and can be seen as a multivariate version of the rank likelihood (Pettitt, 1982; Heller and Qin, 2001), being free of the nuisance parameters for continuous and discrete data. For a more detailed discussion on the extended rank likelihood and sufficient statistics, see Hoff (2007), Section 5.

Hoff (2007) further developed an algorithm to compute the posterior of  $\mathbf{R}$  using the Gibbs sampler with the parameter expansion technique (Liu and Wu, 1999). This algorithm can also be used when observations are missing at random. The algorithm can be easily implemented in the R programming language using the `sbgcop.mcmc` function of the `sbgcop` package.

### 3 Copula estimation under spatial correlation

#### 3.1 Latent models with spatial correlation

Suppose that we obtain observations of mixed outcomes  $\mathbf{y}_{\mathcal{S}}$  equipped with location information  $\mathcal{S}$ , where  $\mathbf{y}_{\mathcal{S}} = (\mathbf{y}(\mathbf{s}_1)^\top, \mathbf{y}(\mathbf{s}_2)^\top, \dots, \mathbf{y}(\mathbf{s}_n)^\top)^\top$ ,  $\mathbf{y}(\mathbf{s}_i) = (y_1(\mathbf{s}_i), y_2(\mathbf{s}_i), \dots, y_p(\mathbf{s}_i))^\top$ ,  $\mathcal{S} = \{\mathbf{s}_1, \mathbf{s}_2, \dots, \mathbf{s}_n\}$ , and  $\mathbf{s}_i$  denotes a two-dimensional vector of longitude and latitude. These observations are characterized by spatial dependence and correlation, and nearby observations have similar properties. In such data, spatial correlations should be adequately considered; otherwise, the estimation of the dependence structure among outcomes would be severely biased. Therefore, we consider a hierarchical spatial model and

latent multivariate Gaussian process. We define the following *spatial Gaussian copula* as a Gaussian copula model combined with a spatial Gaussian process to consider spatial correlation:

$$\mathbf{z}_{\mathcal{S}} = (\mathbf{z}(\mathbf{s}_1)^\top, \mathbf{z}(\mathbf{s}_2)^\top, \dots, \mathbf{z}(\mathbf{s}_n)^\top)^\top \sim N_{pn}(\mathbf{0}, \mathbf{H}(\phi) \otimes \mathbf{R}), \quad (3)$$

where  $\mathbf{z}(\mathbf{s}_i)$  denotes a latent variable equipped with location information  $\mathbf{s}_i$  and  $\mathbf{H}(\phi)$  is a  $n \times n$  matrix whose  $(i, i')$ -element is a valid correlation function  $\rho(\|\mathbf{s}_i - \mathbf{s}_{i'}\|; \phi)$ , such as exponential correlation function  $\exp(-\|\mathbf{s}_i - \mathbf{s}_{i'}\|/\phi)$ , with spatial range parameter  $\phi$ .  $\mathbf{H}(\phi)$  is also interpreted as the correlation matrix of  $\mathbf{z}_{(j)}^{\mathcal{S}} = (z_j(\mathbf{s}_1), z_j(\mathbf{s}_2), \dots, z_j(\mathbf{s}_n))^\top$  with  $\text{Corr}(z_j(\mathbf{s}_i), z_j(\mathbf{s}_{i'})) = \rho(\|\mathbf{s}_i - \mathbf{s}_{i'}\|; \phi)$ . Hereafter, we write  $\mathbf{H}(\phi)$  as  $\mathbf{H}$ , where the dependence on  $\phi$  is implicit, with similar notation for all spatial correlation matrices. The spatial Gaussian copula is identical to that of a multivariate Gaussian process with a correlation structure

$$\text{Corr}(\mathbf{z}(\mathbf{s}_i), \mathbf{z}(\mathbf{s}_{i'})) = \rho(\|\mathbf{s}_i - \mathbf{s}_{i'}\|; \phi) \cdot \mathbf{R},$$

and its correlation structure is known as a separable correlation (e.g., Chapter 9 in [Banerjee et al., 2003](#)).

We consider the extended rank likelihood for the inference of the dependence structure in spatially correlated mixed outcomes, that is, the correlation matrix  $\mathbf{R}$  in the spatial Gaussian copula (3). Observation  $\mathbf{y}_{\mathcal{S}}$  provides us information about the latent variable  $\mathbf{z}_{\mathcal{S}}$  such that, for  $j = 1, 2, \dots, p$ ,  $z_j(\mathbf{s}_i) < z_j(\mathbf{s}_{i'})$  holds when  $y_j(\mathbf{s}_i) < y_j(\mathbf{s}_{i'})$  for an arbitrary pair  $z_j(\mathbf{s}_i)$  and  $z_j(\mathbf{s}_{i'})$  with  $i \neq i'$ , that is,  $\mathbf{z}_{(j)}^{\mathcal{S}}$  must lie in the set

$$D_j = \{\mathbf{z}_{(j)}^{\mathcal{S}} \in \mathbb{R}^n : \max[z_j(\mathbf{s}_k) : y_j(\mathbf{s}_k) < y_j(\mathbf{s}_i)] < z_j(\mathbf{s}_i) < \min[z_j(\mathbf{s}_k) : y_j(\mathbf{s}_i) < y_j(\mathbf{s}_k)]\}.$$

Then, the extended rank likelihood of  $\mathbf{R}$  including the spatial range parameter  $\phi$  under spatial Gaussian copula (3) is given by

$$L(\mathbf{R}, \phi) = \int_{D_1} \int_{D_2} \cdots \int_{D_p} \phi_{pn}(\mathbf{z}_{\mathcal{S}}; \mathbf{0}, \mathbf{H} \otimes \mathbf{R}) d\mathbf{z}_{\mathcal{S}}. \quad (4)$$

Note that this extended rank likelihood considers spatially varying ranks that are not captured by the likelihood in Hoff (2007).

### 3.2 Posterior computation

Extended rank likelihood (4) allows us to develop an effective algorithm for calculating the posteriors of  $\mathbf{R}$  and  $\phi$  using MCMC. The joint posterior of  $\mathbf{R}$ ,  $\phi$ , and  $\mathbf{z}_S$  given  $\mathbf{y}_S$  based on the extended rank likelihood (4), can be expressed as

$$p(\mathbf{R}, \phi, \mathbf{z}_S | \mathbf{y}_S) \propto p(\mathbf{R})p(\phi)\phi_{pn}(\mathbf{z}_S; \mathbf{0}, \mathbf{H} \otimes \mathbf{R}), \quad \mathbf{z}_S \in D_1 \times D_2 \times \cdots \times D_p. \quad (5)$$

Because it is difficult to construct a semi-conjugate prior distribution for  $\mathbf{R}$  due to correlation matrix  $\mathbf{R}$ , we can consider a semi-conjugate prior distribution for the covariance matrix  $\mathbf{V}$  using parameter expansion (Liu and Wu, 1999), as in Hoff (2007). In other words, let  $\mathbf{V}$  follow the inverse-Wishart prior distribution,  $IW(v_0, v_0 \mathbf{V}_0)$ , and use the fact that  $\mathbf{R}$  is equal to the distribution of the correlation matrix, where each element is  $V_{ij}/\sqrt{V_i V_j}$ . The MCMC algorithm for generating the posterior samples of  $\mathbf{R}$ ,  $\phi$ , and  $\mathbf{z}(\mathbf{s}_i)$  for  $i = 1, 2, \dots, n$  is expressed as follows:

- Sampling of  $\mathbf{z}(\mathbf{s}_i)$ : Generate  $\mathbf{z}(\mathbf{s}_i)$  from a  $p$ -dimensional truncated normal distribution,  $TN_p(\boldsymbol{\mu}_{\mathbf{s}_i}, \boldsymbol{\Sigma}_{\mathbf{s}_i}; \boldsymbol{\ell}, \mathbf{u})$ , where

$$\boldsymbol{\mu}_{\mathbf{s}_i} = (\mathbf{H}_{\mathbf{s}_i, \mathcal{S}_{-i}} \mathbf{H}_{\mathcal{S}_{-i}}^{-1} \otimes \mathbf{I}_p) \mathbf{z}_{\mathcal{S}_{-i}}, \quad \boldsymbol{\Sigma}_{\mathbf{s}_i} = (1 - \mathbf{H}_{\mathbf{s}_i, \mathcal{S}_{-i}} \mathbf{H}_{\mathcal{S}_{-i}}^{-1} \mathbf{H}_{\mathbf{s}_i, \mathcal{S}_{-i}}^\top) \mathbf{R},$$

$\mathcal{S}_{-i} = \{\mathbf{s}_{i'} | i \neq i', i' \in \mathbb{N}\}$ ,  $\mathbf{H}_{\mathbf{s}_i, \mathcal{S}_{-i}}$  is the  $(n-1)$ -dimensional cross-correlation row vector between  $\mathbf{z}(\mathbf{s}_i)$  and  $\mathbf{z}_{\mathcal{S}_{-i}}$ ,  $\mathbf{H}_{\mathcal{S}_{-i}}$  is the  $(n-1) \times (n-1)$  correlation matrix of  $\mathbf{z}_{\mathcal{S}_{-i}}$ , and the  $j$ -th element of  $p$ -dimensional vectors  $\boldsymbol{\ell}$  and  $\mathbf{u}$  are

$$\ell_j = \max[z_j(\mathbf{s}_k) : y_j(\mathbf{s}_k) < y_j(\mathbf{s}_i)] \quad \text{and} \quad u_j = \min[z_j(\mathbf{s}_k) : y_j(\mathbf{s}_i) < y_j(\mathbf{s}_k)],$$

denoting the lower and upper bounds of the truncated normal distribution in each dimension.

- Sampling  $\mathbf{R}$ : Generate  $\mathbf{V}$  from  $IW(v_0 + n, v_0 \mathbf{V}_0 + \sum_{i=1}^n h_i^{-1} [\mathbf{z}(\mathbf{s}_i) - \bar{\mathbf{z}}_i][\mathbf{z}(\mathbf{s}_i) - \bar{\mathbf{z}}_i]^\top)$ ,



where

$$h_i = 1 - \mathbf{H}_{\mathbf{s}_i, \mathcal{C}_i} \mathbf{H}_{\mathcal{C}_i}^{-1} \mathbf{H}_{\mathbf{s}_i, \mathcal{C}_i}^\top, \quad \bar{\mathbf{z}}_i = (\mathbf{H}_{\mathbf{s}_i, \mathcal{C}_i} \mathbf{H}_{\mathcal{C}_i}^{-1} \otimes \mathbf{I}_p) \mathbf{z}_{\mathcal{C}_i},$$

$\mathcal{C}_i = \{\mathbf{s}_{i'} | i' < i, i' \in \mathbb{N}\}$ ,  $\mathbf{H}_{\mathbf{s}_i, \mathcal{C}_i}$  is the  $c_i$ -dimensional cross-correlation row vector between  $\mathbf{z}(\mathbf{s}_i)$  and  $\mathbf{z}_{\mathcal{C}_i}$  with  $c_i = |\mathcal{C}_i|$ , and  $\mathbf{H}_{\mathcal{C}_i}$  is the  $c_i \times c_i$  correlation matrix of  $\mathbf{z}_{\mathcal{C}_i}$ , and transform  $\mathbf{R}_{ij} = \mathbf{V}_{ij} / \sqrt{\mathbf{V}_i \mathbf{V}_j}$ .

- Sampling  $\phi$ : The full conditional of  $\phi$  is proportional to

$$|\mathbf{H}|^{-p/2} \exp \left\{ -\frac{1}{2} \sum_{i=1}^n h_i^{-1} [\mathbf{z}(\mathbf{s}_i) - \bar{\mathbf{z}}_i]^\top \mathbf{V}^{-1} [\mathbf{z}(\mathbf{s}_i) - \bar{\mathbf{z}}_i] \right\}.$$

A random-walk Metropolis-Hastings is used to sample from this distribution.

The posterior computation above involves sampling from a  $p$ -dimensional truncated normal (tMVN) distribution. For scalable posterior computation, it is important to discuss sampling from tMVN. Several approaches exist for sampling from a tMVN distribution, including sequential sampling from conditionally univariate truncated normal distributions (Geweke, 1991; Kotecha and Djuric, 1999; Damien and Walker, 2001), the Hamiltonian Markov chain algorithm (Pakman and Paninski, 2014), the minimax tilting accept-reject algorithm (Botev, 2017), and an approximate sampling algorithm based on the cumulative distribution function of the standard logistic distribution (Souris et al., 2018). Although the details are omitted here, we performed simulations to identify the most efficient tMVN sampling algorithm for our posterior computation, except for Pakman and Paninski (2014), which required tuning. Consequently, because there were no notable changes in the mixing properties, we adopted the algorithm of Botev (2017), which is easier to implement using the R package `TruncatedNormal` (Botev and Belzile, 2021). However, when the number of dimensions exceeds 100, the acceptance probability decreases, and the algorithm slows down. In such cases, we should consider using other algorithms, such as an approximate sampling algorithm that uses the probit function for sampling from the tMVN.

### 3.3 Scalable posterior computation under large spatial data

The Gaussian process has gained considerable popularity in spatial modeling owing to its excellent properties; however, it suffers from computational intractability, for example, in

matrix operations and memory related to the covariance matrix (or correlation matrix) (Heaton et al., 2019; Liu et al., 2020). The inference algorithm proposed in the previous section is no exception. In each iteration of the MCMC, the inverse of the spatial correlation matrix  $\mathbf{H}$  in the Gaussian process and related matrix operations are required for every update of  $\mathbf{z}(\mathbf{s}_i)$ ,  $\mathbf{R}$  and  $\phi$ . Therefore, in the current algorithm, even with a dataset of a few thousand observations, it would take more than one day of computation time with a standard laptop and, in some cases, memory explosion would occur, rendering the analysis impossible.

To address this problem, we employ the nearest-neighbor Gaussian process (NNGP) proposed by Datta et al. (2016) for  $\mathbf{z}_S$  with a multivariate normal distribution and sparse precision matrix defined as

$$p(\mathbf{z}_S) = \prod_{i=1}^n \phi_p(\mathbf{z}(\mathbf{s}_i); \mathbf{B}_{\mathbf{s}_i} \mathbf{z}_{\mathcal{N}_i}, F_{\mathbf{s}_i} \mathbf{R}),$$

where

$$\mathbf{B}_{\mathbf{s}_i} = \mathbf{H}_{\mathbf{s}_i, \mathcal{N}_i} \mathbf{H}_{\mathcal{N}_i}^{-1} \otimes \mathbf{I}_p, \quad F_{\mathbf{s}_i} = 1 - \mathbf{H}_{\mathbf{s}_i, \mathcal{N}_i} \mathbf{H}_{\mathcal{N}_i}^{-1} \mathbf{H}_{\mathbf{s}_i, \mathcal{N}_i}^\top,$$

$\mathcal{N}_i = \{\mathbf{s}_{i'} | i' \text{ is an index of } m\text{-nearest neighbor of } \mathbf{s}_i\}$ ,  $\mathbf{H}_{\mathbf{s}_i, \mathcal{N}_i}$  is the  $n_i$ -dimensional cross-correlation row vector between  $\mathbf{z}(\mathbf{s}_i)$  and  $\mathbf{z}_{\mathcal{N}_i}$  with  $n_i = |\mathcal{N}_i| (\leq m)$ , and  $\mathbf{H}_{\mathcal{N}_i}$  is the  $n_i \times n_i$  correlation matrix of  $\mathbf{z}_{\mathcal{N}_i}$ . Under NNGP, which is a type of Vecchia approximation (Vecchia, 1988), the conditional distribution of  $\mathbf{z}(\mathbf{s}_i)$  can be expressed as

$$p(\mathbf{z}(\mathbf{s}_i) | \mathbf{z}_{S-i}) = p(\mathbf{z}(\mathbf{s}_i) | \mathbf{z}_{\mathcal{D}_i}),$$

where  $\mathcal{D}_i = \{\mathbf{s}_{i'} | \mathbf{s}_i \in \mathcal{N}_{i'}\} \cup \mathcal{N}_i$  since  $(\mathbf{z}(\mathbf{s}_i), \mathbf{z}_{\mathcal{D}_i}) \perp\!\!\!\perp \mathbf{z}_{S-i \setminus \mathcal{D}_i}$ . Then, the MCMC algorithm for generating posterior samples of  $\mathbf{R}$ ,  $\phi$ , and  $\mathbf{z}(\mathbf{s}_i)$  is provided as follows:

- Sampling of  $\mathbf{z}(\mathbf{s}_i)$ : Generate  $\mathbf{z}(\mathbf{s}_i)$  from a  $p$ -dimensional truncated normal distribution,  $TN_p(\tilde{\boldsymbol{\mu}}_{\mathbf{s}_i}, \tilde{\boldsymbol{\Sigma}}_{\mathbf{s}_i}; \boldsymbol{\ell}, \mathbf{u})$ , where

$$\tilde{\boldsymbol{\mu}}_{\mathbf{s}_i} = (\mathbf{H}_{\mathbf{s}_i, \mathcal{D}_i} \mathbf{H}_{\mathcal{D}_i}^{-1} \otimes \mathbf{I}_p) \mathbf{z}_{\mathcal{D}_i}, \quad \tilde{\boldsymbol{\Sigma}}_{\mathbf{s}_i} = (1 - \mathbf{H}_{\mathbf{s}_i, \mathcal{D}_i} \mathbf{H}_{\mathcal{D}_i}^{-1} \mathbf{H}_{\mathbf{s}_i, \mathcal{D}_i}^\top) \mathbf{R},$$

$\mathbf{H}_{\mathbf{s}_i, \mathcal{D}_i}$  is the  $d_i$ -dimensional cross-correlation row vector between  $\mathbf{z}(\mathbf{s}_i)$  and  $\mathbf{z}_{\mathcal{D}_i}$  with

$d_i = |\mathcal{D}_i|$ ,  $\mathbf{H}_{\mathcal{D}_i}$  is the  $d_i \times d_i$  correlation matrix of  $\mathbf{z}_{\mathcal{D}_i}$ .

- Sampling  $\mathbf{R}$ : Generate  $\mathbf{V}$  from

$$IW \left( v_0 + n, v_0 \mathbf{V}_0 + \sum_{i=1}^n F_{\mathbf{s}_i}^{-1} [\mathbf{z}(\mathbf{s}_i) - \mathbf{B}_{\mathbf{s}_i} \mathbf{z}_{\mathcal{N}_i}] [\mathbf{z}(\mathbf{s}_i) - \mathbf{B}_{\mathbf{s}_i} \mathbf{z}_{\mathcal{N}_i}]^\top \right),$$

and transform  $\mathbf{R}_{ij} = \mathbf{V}_{ij} / \sqrt{\mathbf{V}_i \mathbf{V}_j}$ .

- Sampling  $\phi$ : The full conditional of  $\phi$  is proportional to

$$|\mathbf{H}|^{-p/2} \exp \left\{ -\frac{1}{2} \sum_{i=1}^n F_{\mathbf{s}_i}^{-1} [\mathbf{z}(\mathbf{s}_i) - \mathbf{B}_{\mathbf{s}_i} \mathbf{z}_{\mathcal{N}_i}]^\top \mathbf{V}^{-1} [\mathbf{z}(\mathbf{s}_i) - \mathbf{B}_{\mathbf{s}_i} \mathbf{z}_{\mathcal{N}_i}] \right\}.$$

A random-walk Metropolis-Hastings is used to sample from this distribution.

In the calculation of  $\tilde{\boldsymbol{\mu}}_{\mathbf{s}_i}$  and  $\tilde{\boldsymbol{\Sigma}}_{\mathbf{s}_i}$  in the full conditional of  $\mathbf{z}(\mathbf{s}_i)$ ,  $(n-1)$ -dimensional matrix operations are required with the full Gaussian process, as seen in Section 3.2, but with the NNGP, we only need a  $d_i$  ( $< (n-1)$ )-dimension matrix operations at most. Moreover, because only  $m$  ( $\ll n$ )-dimensional matrix operations are required to sample  $\mathbf{R}$  and  $\phi$  from their full conditional, computational cost can be considerably reduced compared to the full Gaussian process. Although the value of  $m$  needs to be chosen based on the available computational resources, in many situations, relatively small values of  $m$  (e.g.,  $m < 100$ ) can achieve high accuracy. For a detailed discussion, see, for example, [Katzfuss and Guinness \(2021\)](#). In practice, in our method, even with a sample from a few hundreds to thousands of observations, the estimation accuracy remains almost the same, whereas the computation time is significantly reduced compared to the full Gaussian process.

## 4 Simulation study

Using a simulation study, this section demonstrates that the proposed approach successfully accounts for spatial correlation and correctly infers the dependence structure among spatially correlated multivariate mixed outcomes, including a comparison with [Hoff \(2007\)](#). To this end, we consider spatial Gaussian copula (3) with  $n \in \{50, 500, 1000\}$  and  $p \in \{6, 9\}$ , where  $\phi \in \{0.05, 0.25, 0.5\}$  and  $\mathbf{R}_{12} = 0.5$ ,  $\mathbf{R}_{14} = 0.3$ ,  $\mathbf{R}_{15} = 0.2$ ,  $\mathbf{R}_{23} = -0.2$ ,  $\mathbf{R}_{24} = -0.3$ ,  $\mathbf{R}_{35} = 0.4$ ,  $\mathbf{R}_{45} = -0.5$ , and all others to zero for  $j < j'$ . Location infor-

mation  $s_{i1}$  and  $s_{i2}$  are generated from  $\text{Unif}(0, 1)$ . Using the spatial Gaussian copula, we generate a simulated dataset based on [Smith \(2021\)](#):

Step 1. Calculate spatial correlation matrix  $\mathbf{H}$  with location information  $\mathbf{s}_i = (s_{i1}, s_{i2})^\top$ .

Step 2. Generate latent variables  $\mathbf{z}_S$  from multivariate Gaussian process (3).

Step 3. Calculate  $y_j(\mathbf{s}_i) = F_j^{-1}[\Phi(z_j(\mathbf{s}_i))]$ , where  $F_j$  is a specified cumulative distribution function for  $j = 1, 2, \dots, p$ .

In our simulation setting,  $y_1(\mathbf{s}_i) \sim \text{Bernoulli}(0.5)$ ,  $y_2(\mathbf{s}_i) \sim \text{Poi}(15)$ ,  $y_3(\mathbf{s}_i) \sim \text{Poi}(5)$ ,  $y_4(\mathbf{s}_i) \sim \text{OrderedCategorical}(0.3, 0.15, 0.1, 0.25, 0.2)$ , and all other  $y_j(\mathbf{s}_i)$ s are generated from normal distributions.

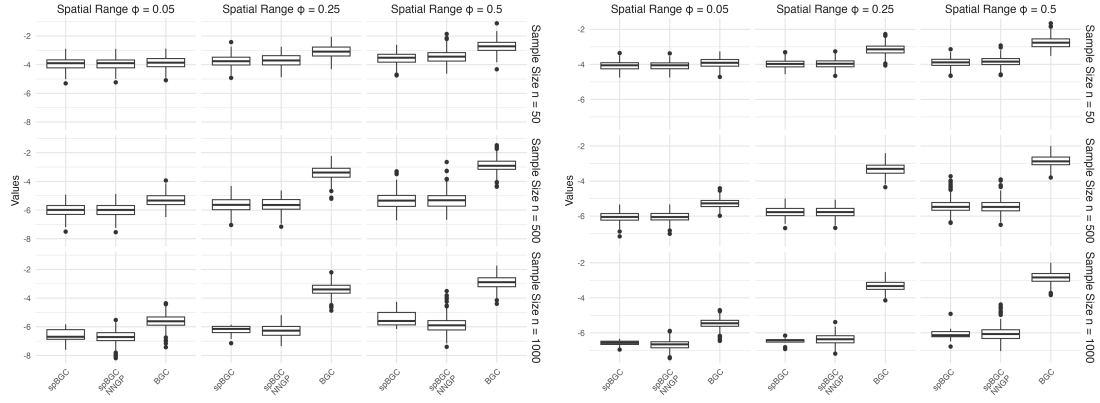
For the simulated dataset, we apply the proposed and [Hoff \(2007\)](#) methods, denoted as spBGC and BGC, respectively. In doing so, we use 2000 draws for the posterior computation after discarding the first 1000 draws as burn-in, and we set  $IW(p+2, (p+2)\mathbf{I})$  prior for  $\mathbf{V}$  as a prior for  $\mathbf{V}$ . We compute posterior medians  $\{\hat{\mathbf{R}}_{jj'}\}_{j < j'}$  as point estimates of  $\mathbf{R}_{jj'}$  for  $j < j'$  and evaluate their performance by the mean squared error (MSE), defined as  $q^{-1} \sum_{j < j'} (\hat{\mathbf{R}}_{jj'} - \mathbf{R}_{jj'})^2$  where  $q = p(p-1)/2$ . We also compute 95% credible intervals and calculate coverage probabilities (CP) and average lengths (AL), defined as  $q^{-1} \sum_{j < j'} I(\mathbf{R}_{jj'} \in \text{CI}_{jj'})$  and  $q^{-1} \sum_{j < j'} |\text{CI}_{jj'}|$ , respectively, where  $I(\cdot)$  is the indicator function and  $\text{CI}_{jj'}$  is the 95% credible interval of  $\mathbf{R}_{jj'}$ . These values are averaged over 300 replications of the simulated datasets.

Furthermore, we determine the advantages of using NNGP in the spBGC. Hereafter, we denote spBGCNNGP to clarify its use. As described below, although spBGCNNGP can considerably reduce the computation time compared to spBGC, even for a sample size of 500, its estimation accuracy remains almost the same. Because spBGC requires considerable time per simulation when the sample size is 1000, we evaluate the performance of spBGC with only 10 iterations in this setting. This simulation study was conducted on an Apple Mac Studio with an Apple M1 Ultra chip, using programming language R ([R Core Team, 2024](#)).

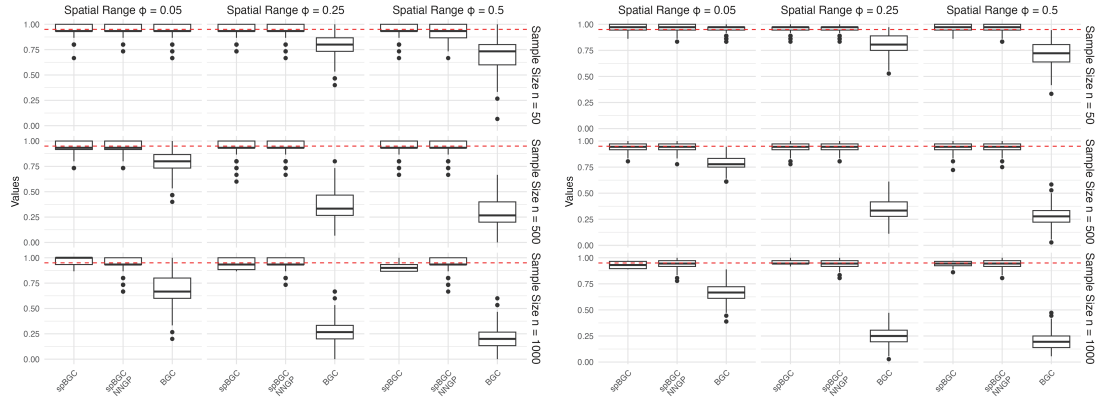
The simulation results presented in Figure 2 and Tables 1–4 clearly demonstrate the superior performance of our proposed methods, spBGC, and its computationally efficient

version, spBGCNNGP, compared with the existing BGC method. Figure 2(a) and Table 1 show that both spBGC and spBGCNNGP achieve significantly lower MSEs than BGC across all scenarios. This difference becomes more pronounced as spatial correlation ( $\phi$ ) increases, highlighting the ability of the proposed method to effectively account for spatial dependence. The CPs displayed in Figure 2(b) and Table 2 reveal that spBGC and spBGCNNGP consistently maintain CPs close to the nominal 95% level. By contrast, BGC coverage deteriorates substantially as the spatial correlation strengthens, often falling well below the desired level. This underscores the reliability of the proposed method for providing accurate credible intervals. The ALs of the credible intervals, as shown in Figure 2(c) and Table 3, indicate that spBGC and spBGCNNGP achieve high coverage probabilities, while maintaining reasonably narrow interval widths. Balancing coverage and precision is crucial for practical applications. Most notably, Table 4 highlights the computational efficiency of spBGCNNGP. As the sample size increases, the time savings offered by spBGCNNGP become increasingly significant. For instance, for  $n = 1000$ , spBGCNNGP completes the computation in approximately one-sixth of the time required by the spBGC, while maintaining a comparable estimation accuracy.

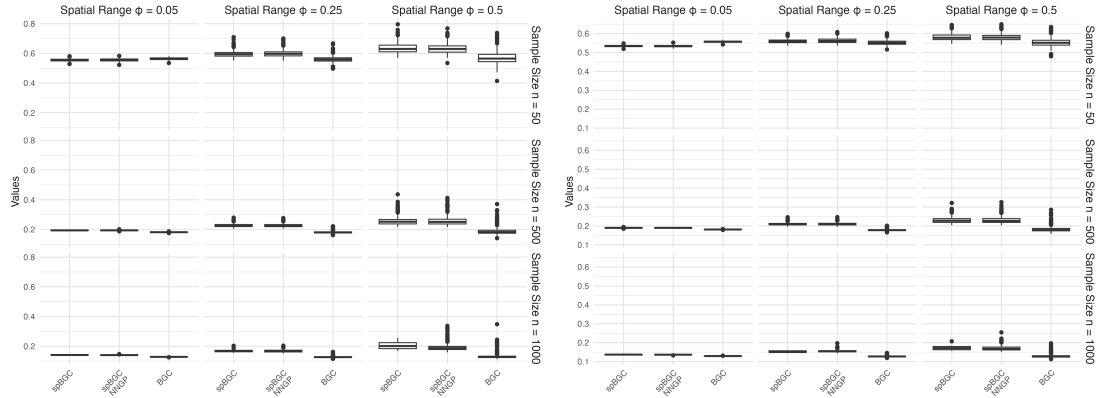
These results collectively demonstrate that the proposed methods, particularly the spBGCNNGP, offer a powerful combination of estimation accuracy and computational efficiency for analyzing spatially correlated multivariate mixed outcomes. The ability of spBGCNNGP to significantly reduce computation time without sacrificing estimation quality is particularly valuable for large-scale spatial datasets, which are becoming increasingly common in various research areas. By employing the spBGCNNGP, researchers and practitioners can perform high-precision estimations of spatial dependence structures on datasets that were previously computationally infeasible. This opens new possibilities for in-depth spatial analyses across a wide range of applications, from environmental science to epidemiology. In conclusion, the spBGCNNGP is a robust and efficient tool for analyzing spatially correlated multivariate mixed outcomes, offering an optimal balance between accuracy and computational efficiency. Its ability to handle large-scale spatial datasets with high precision renders it an invaluable asset for researchers studying complex spatial datasets.



(a) The logarithm of the MSEs for  $p = 6$  (left) and  $p = 9$  (right)



(b) The CPs for  $p = 6$  (left) and  $p = 9$  (right)



(c) The ALs for  $p = 6$  (left) and  $p = 9$  (right)

**Figure 2:** Comparisons of the logarithm of the MSEs (a), CPs (b), and ALs (c) for the spBGC, spBGCNNGP, and BGC under varying sample sizes ( $n \in \{50, 500, 1000\}$ ) and spatial range parameters ( $\phi \in \{0.05, 0.25, 0.5\}$ ). The red dashed line in the CP graphs indicates the target coverage probability of 0.95. Each figure shows results for the number of outcomes  $p = 6$  on the left and  $p = 9$  on the right.

**Table 1:** Comparisons of the logarithm of the MSEs for the spBGC, spBGCNNGP, and BGC under varying sample sizes ( $n \in \{50, 500, 1000\}$ ) and spatial range parameters ( $\phi \in \{0.05, 0.25, 0.5\}$ ). The values represent average  $\log(\text{MSE})$ s from 300 calculations, with standard errors between parentheses.

(a) Number of outcomes $p = 6$				(b) Number of outcomes $p = 9$			
	$\phi$				$\phi$		
	0.05	0.25	0.50		0.05	0.25	0.50
$n = 50$				$n = 50$			
spBGC	−3.939 (0.024)	−3.749 (0.024)	−3.559 (0.024)	spBGC	−4.079 (0.015)	−3.978 (0.014)	−3.894 (0.015)
spBGCNNGP	−3.938 (0.023)	−3.705 (0.024)	−3.438 (0.027)	spBGCNNGP	−4.084 (0.015)	−3.967 (0.014)	−3.838 (0.017)
BGC	−3.861 (0.024)	−3.096 (0.026)	−2.730 (0.026)	BGC	−3.925 (0.016)	−3.139 (0.018)	−2.752 (0.020)
$n = 500$				$n = 500$			
spBGC	−6.007 (0.026)	−5.643 (0.028)	−5.317 (0.034)	spBGC	−6.046 (0.017)	−5.762 (0.016)	−5.424 (0.023)
spBGCNNGP	−6.017 (0.026)	−5.641 (0.028)	−5.309 (0.035)	spBGCNNGP	−6.044 (0.016)	−5.764 (0.017)	−5.441 (0.023)
BGC	−5.323 (0.027)	−3.395 (0.028)	−2.889 (0.026)	BGC	−5.268 (0.016)	−3.316 (0.019)	−2.857 (0.019)
$n = 1000$				$n = 1000$			
spBGC	−6.608 (0.160)	−6.288 (0.134)	−5.428 (0.199)	spBGC	−6.596 (0.063)	−6.485 (0.072)	−6.053 (0.156)
spBGCNNGP	−6.703 (0.026)	−6.289 (0.024)	−5.870 (0.034)	spBGCNNGP	−6.673 (0.015)	−6.365 (0.018)	−6.032 (0.024)
BGC	−5.620 (0.027)	−3.396 (0.027)	−2.904 (0.028)	BGC	−5.465 (0.016)	−3.324 (0.017)	−2.834 (0.019)

**Table 2:** Comparison of CPs for the spBGC, spBGCNNGP, and BGC across varying sample sizes ( $n \in \{50, 500, 1000\}$ ) and spatial range parameters ( $\phi \in \{0.05, 0.25, 0.5\}$ ). The values represent average CPs from 300 calculations, with standard errors between parentheses.

(a) Number of outcomes $p = 6$				(b) Number of outcomes $p = 9$			
	$\phi$				$\phi$		
	0.05	0.25	0.50		0.05	0.25	0.50
$n = 50$				$n = 50$			
spBGC	0.950 (0.003)	0.948 (0.003)	0.944 (0.004)	spBGC	0.962 (0.002)	0.962 (0.002)	0.963 (0.002)
spBGCNNGP	0.954 (0.003)	0.947 (0.004)	0.933 (0.004)	spBGCNNGP	0.962 (0.002)	0.961 (0.002)	0.961 (0.002)
BGC	0.943 (0.004)	0.797 (0.008)	0.722 (0.009)	BGC	0.954 (0.002)	0.810 (0.005)	0.711 (0.006)
$n = 500$				$n = 500$			
spBGC	0.941 (0.004)	0.944 (0.004)	0.947 (0.004)	spBGC	0.945 (0.002)	0.943 (0.002)	0.941 (0.002)
spBGCNNGP	0.943 (0.004)	0.943 (0.004)	0.940 (0.004)	spBGCNNGP	0.943 (0.002)	0.944 (0.002)	0.942 (0.002)
BGC	0.789 (0.007)	0.360 (0.008)	0.292 (0.008)	BGC	0.787 (0.004)	0.349 (0.005)	0.278 (0.005)
$n = 1000$				$n = 1000$			
spBGC	0.967 (0.015)	0.940 (0.018)	0.907 (0.015)	spBGC	0.931 (0.011)	0.956 (0.007)	0.936 (0.012)
spBGCNNGP	0.946 (0.004)	0.944 (0.003)	0.942 (0.004)	spBGCNNGP	0.941 (0.002)	0.945 (0.002)	0.938 (0.002)
BGC	0.691 (0.008)	0.262 (0.007)	0.209 (0.007)	BGC	0.669 (0.005)	0.256 (0.005)	0.205 (0.005)



**Table 3:** Comparison of ALs for the spBGC, spBGCNNGP, and BGC across varying sample sizes ( $n \in \{50, 500, 1000\}$ ) and spatial range parameters ( $\phi \in \{0.05, 0.25, 0.5\}$ ). The values represent average ALs from 300 calculations, with standard errors between parentheses.

(a) Number of outcomes $p = 6$				(b) Number of outcomes $p = 9$			
	$\phi$				$\phi$		
	0.05	0.25	0.50		0.05	0.25	0.50
$n = 50$				$n = 50$			
spBGC	0.555 (0.001)	0.596 (0.001)	0.635 (0.002)	spBGC	0.534 (0.000)	0.560 (0.001)	0.581 (0.001)
spBGCNNGP	0.556 (0.001)	0.600 (0.001)	0.633 (0.002)	spBGCNNGP	0.534 (0.000)	0.563 (0.001)	0.581 (0.001)
BGC	0.563 (0.000)	0.559 (0.001)	0.572 (0.003)	BGC	0.557 (0.000)	0.552 (0.001)	0.554 (0.001)
$n = 500$				$n = 500$			
spBGC	0.194 (0.000)	0.227 (0.001)	0.257 (0.002)	spBGC	0.190 (0.000)	0.210 (0.000)	0.232 (0.001)
spBGCNNGP	0.194 (0.000)	0.227 (0.001)	0.258 (0.002)	spBGCNNGP	0.190 (0.000)	0.211 (0.000)	0.232 (0.001)
BGC	0.181 (0.000)	0.181 (0.000)	0.188 (0.002)	BGC	0.181 (0.000)	0.178 (0.000)	0.183 (0.001)
$n = 1000$				$n = 1000$			
spBGC	0.140 (0.001)	0.170 (0.005)	0.205 (0.009)	spBGC	0.137 (0.000)	0.152 (0.001)	0.174 (0.005)
spBGCNNGP	0.140 (0.000)	0.167 (0.001)	0.192 (0.001)	spBGCNNGP	0.136 (0.000)	0.155 (0.000)	0.171 (0.001)
BGC	0.128 (0.000)	0.127 (0.000)	0.132 (0.001)	BGC	0.129 (0.000)	0.128 (0.000)	0.130 (0.001)

**Table 4:** Comparison of execution times for the spBGC and spBGCNNGP across varying sample sizes ( $n \in \{50, 500, 1000\}$ ) and spatial range parameters ( $\phi \in \{0.05, 0.25, 0.5\}$ ). The values represent average execution times from 300 calculations, with standard errors between parentheses.

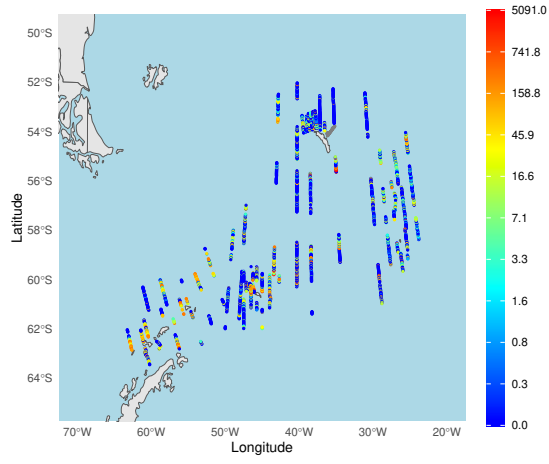
(a) Number of outcomes $p = 6$				(b) Number of outcomes $p = 9$			
	$\phi$				$\phi$		
	0.05	0.25	0.50		0.05	0.25	0.50
$n = 50$				$n = 50$			
spBGC	90.673 (0.043)	90.227 (0.052)	89.660 (0.186)	spBGC	110.163 (0.056)	109.461 (0.085)	108.997 (0.238)
spBGC NNGP	90.310 (0.051)	89.891 (0.047)	89.423 (0.171)	spBGC NNGP	109.689 (0.055)	109.056 (0.082)	108.741 (0.212)
$n = 500$				$n = 500$			
spBGC	1599.052 (0.542)	1576.924 (0.587)	1573.239 (1.952)	spBGC	1838.138 (0.556)	1813.001 (0.571)	1810.859 (0.754)
spBGC NNGP	867.857 (0.384)	845.439 (0.431)	842.481 (1.107)	spBGC NNGP	1094.614 (0.471)	1070.287 (0.535)	1066.730 (0.632)
$n = 1000$				$n = 1000$			
spBGC	12341.233 (24.464)	12223.131 (18.736)	12331.789 (17.548)	spBGC	12882.985 (21.570)	12966.792 (18.202)	12804.945 (20.865)
spBGC NNGP	2010.361 (2.109)	1953.853 (1.870)	1965.046 (3.196)	spBGC NNGP	2541.520 (1.985)	2503.737 (1.859)	2489.028 (3.157)

## 5 Real data applications

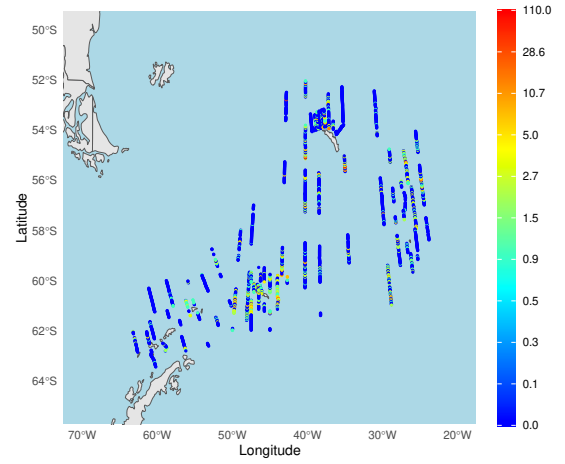
We applied our method to the visual sightings of fin whales from line transect surveys in the Southern Ocean. Visual observations were performed on three of the six vessels participating in the 2019 Area 48 Survey for Antarctic krill (Krafft et al., 2021): R/V Kronprins Haakon (KPH), F/V Cabo de Hornos (CDH), and RRS Discovery (DIS). The details of the observation methods and protocols for fin whales can be found in Biuw et al. (2024). The observed data in this study are the number of fin whales and the acoustic data of krill from vessels operating along the transects. Krill biomass estimates were recalculated based on the acoustic data (details in the Supplementary Material of Krafft et al., 2021). The observation transects were split into 1-nm long segments, resulting in 3,833 segments based on 42 transects, and the number of fin sightings (groups and

individuals) and krill biomass were summarized for each segment.

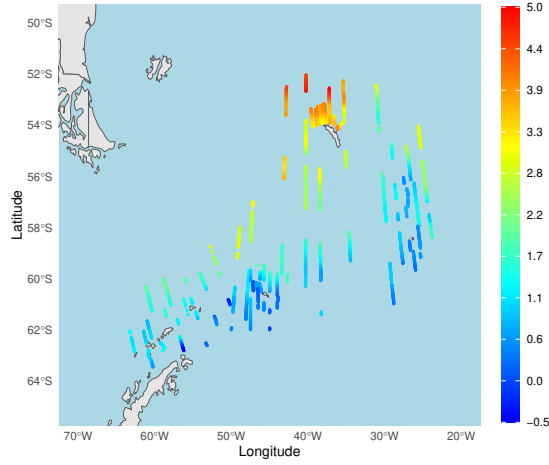
We also included surface temperature (Celsius) and water depth (m) for a 1-nm segment to investigate the association of environmental data with the biological community. Figure 3 shows the spatial plots for krill biomass (Krill), sighting data of fin whales (Whale), surface temperature (SST), depth data (Depth), slope of the depth (Slope), and gradient surface temperature (SST.grd). Brighter/darker dots' colors for surface temperature and water depth indicate higher/lower temperatures and shallower/deeper water depths, respectively. Water depth data were obtained from the ETOPO 1 bathymetric dataset, available at <https://www.ncei.noaa.gov/products/etopo-global-relief-model>. Data were extracted for the middle position of each 1-nm segment throughout the survey tracks. Data on SST were obtained from the OISST dataset, available at <https://www.ncei.noaa.gov/products/optimum-interpolation-sst>, being extracted in the same way as for depth data. The slope of the depth is the maximum rate of change in depth from that cell to its neighbors, calculated using the *Slope* tool of the Surface toolset in ArcGIS (<https://desktop.arcgis.com/en/arcmap/10.3/tools/spatial-analyst-toolbox/an-overview-of-the-surface-tools.htm>). The lower the slope value is, the flatter is the terrain, and vice versa. The gradient surface temperature was calculated using the *Slope* applied to the SST.



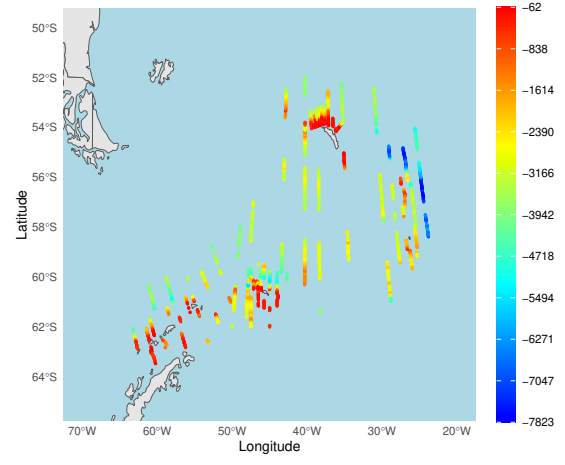
(a) Krill



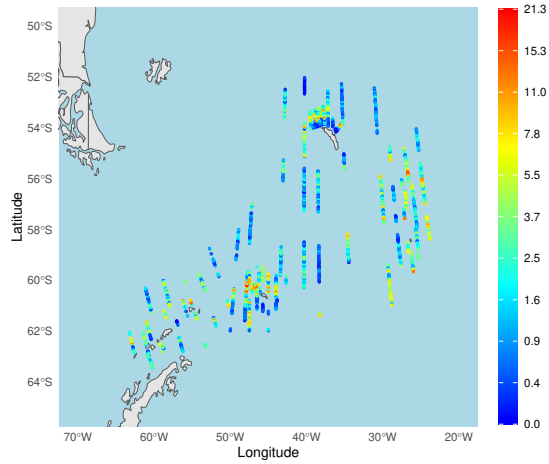
(b) Whale



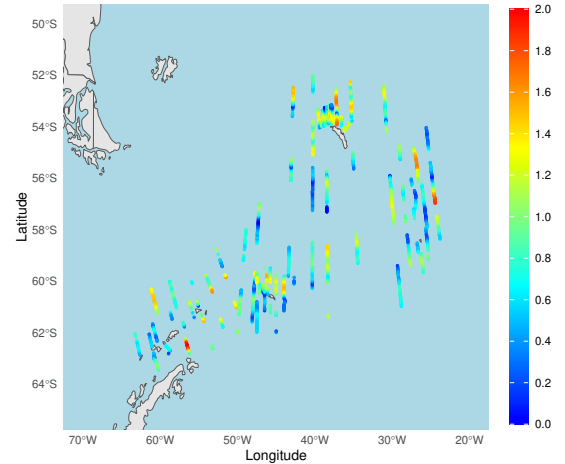
(c) SST



(d) Depth



(e) Slope



(f) SST.grd

**Figure 3:** Spatial plots for krill biomass (Krill), sighting data of fin whales (Whale), surface temperature (SST), depth data (Depth), slope of the depth (Slope), and gradient surface temperature (SST.grd).

We are interested in the dependence structure of krill biomass and sighting data of fin whales, and that of each of these outcomes and environmental factors (SST, Depth, Slope, and SST.grd). Therefore, this application focuses on the posterior inference of these dependence structures. We compare the results of the proposed method (spBGC) with those of Hoff (2007)’s method (BGC), which does not consider spatial correlation. Before the comparison, we examine the mixing properties of spBGC. Using an  $IW(p+2, (p+2)\mathbf{I})$  prior, that is,  $IW(8, 8\mathbf{I})$  for  $\mathbf{V}$ , we conduct MCMC with 25,000 iterations, discarding the first 5,000 as burn-in and retaining every 10th sample from the remaining chain, yielding 2,000 samples for posterior calculations. Figure 4 presents the mixing and autocorrelation results for the correlation coefficients of interest. From these figures, the mixing properties of our spBGC algorithm are quite satisfactory, that is, convergence to stationarity appears and the autocorrelation at lag-20 is close to zero for most elements.

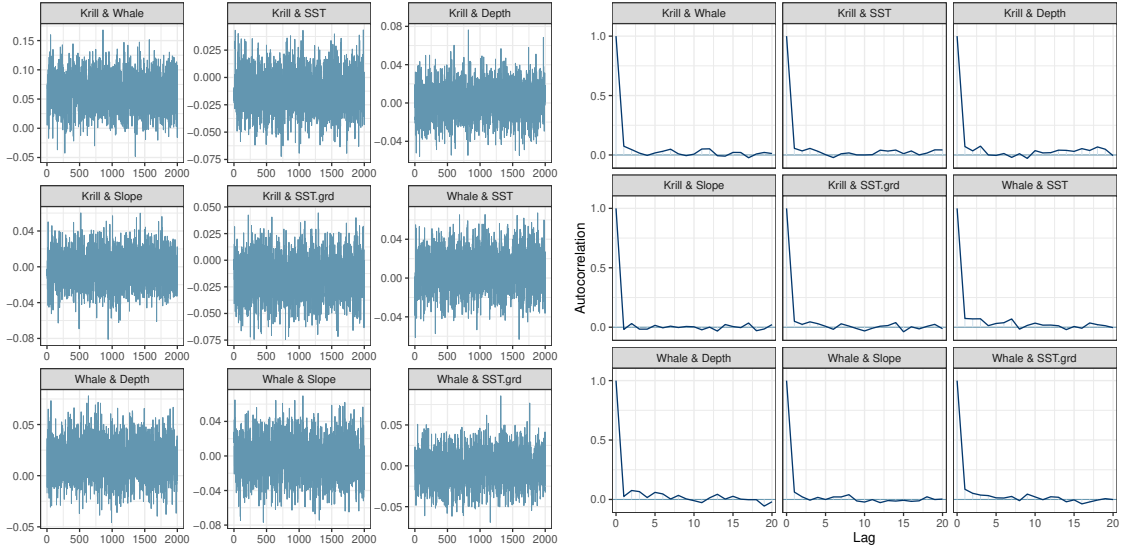


**Figure 4:** Trace plots and autocorrelation of posterior draws of the correlation coefficients based on the spBGC algorithm.

Based on 2,000 posterior draws, we compute the posterior medians and 95% credible intervals of the correlations between the variables, as shown in Figure 5 and Tables 5 and 6. The results reveal that spBGC and BGC yield markedly different estimates for several correlations. In particular, spBGC intervals suggest that Krill has no strong positive or negative correlation with outcomes other than Whale. By contrast, BGC intervals exclude zero for all Krill- and Whale-related outcomes except Depth. Turning to the structure of conditional independence, we also examined partial correlations. Figure 5 and Tables

5 and 6 also show that these partial correlation estimates differ substantially between spBGC and BGC. Notably, the 95% credible intervals from spBGC exclude only zero for the partial correlation between Krill and Whale, whereas the BGC identifies additional pairs with non-zero partial correlations.

As a related analysis, Solvang et al. (2024) applied standard generalized linear models to the same dataset. The results showed a significant positive association between Krill and Whale. Furthermore, the estimated coefficients on SST were significantly negative, while those on Slope were positive for both Krill and Whale. These results are similar to those obtained for the BGC, possibly because neither BGC nor the generalized linear models account for spatial correlation. In contrast, by using the proposed spBGC that considers spatial correlation, we identified relationships that slightly differ from previous findings. This may provide new interpretations of the relationships between the variables.

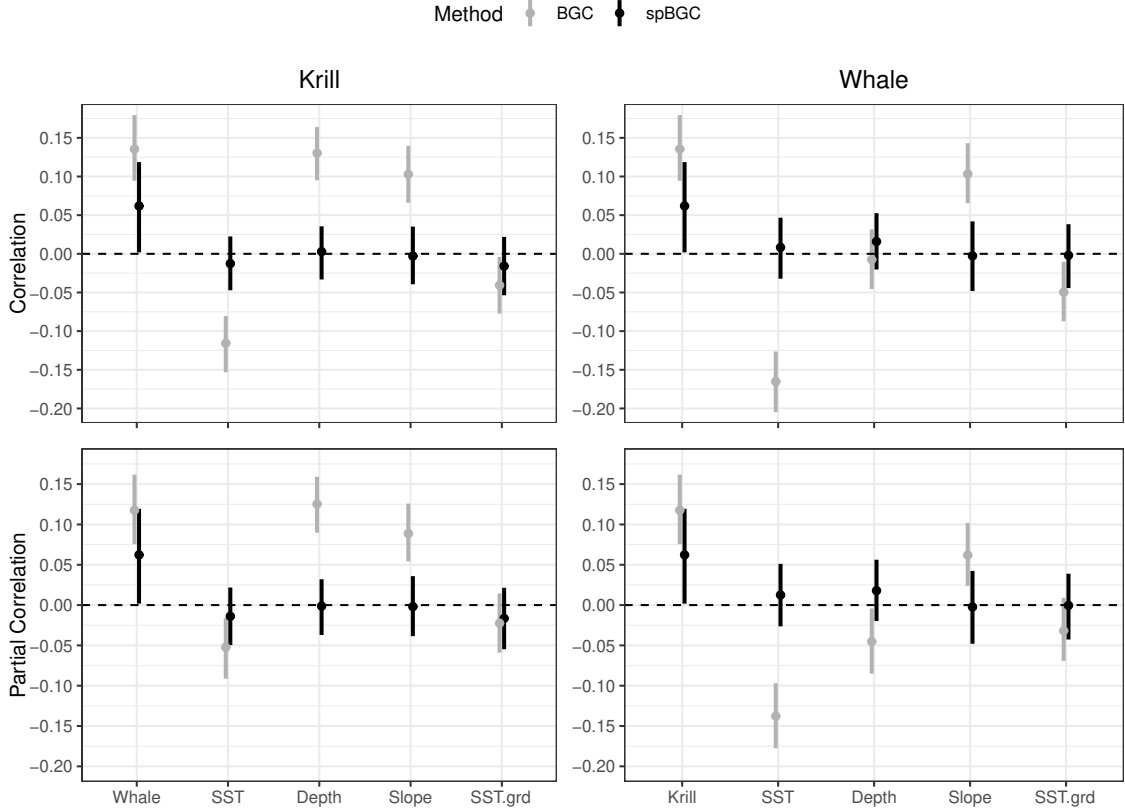


**Figure 5:** 95% credible intervals with posterior medians (●) of the correlation coefficients (upper) and partial correlations (bottom) based on the proposed method, spBGC (black), and Hoff (2007)'s one, BGC (grey).

**Table 5:** 2.5%, 50%, and 97.5% posterior quantiles of the correlation coefficients and partial correlations based on the proposed method, spBGC.

(a) Krill				(b) Whale			
	2.5%	Median	97.5%		2.5%	Median	97.5%
<b>Correlation</b>				<b>Correlation</b>			
Whale	0.0019	0.0619	0.1187	Krill	0.0019	0.0619	0.1187
SST	-0.0472	-0.0126	0.0225	SST	-0.0322	0.0083	0.0467
Depth	-0.0332	0.0028	0.0356	Depth	-0.0202	0.0159	0.0526
Slope	-0.0393	-0.0029	0.0352	Slope	-0.0481	-0.0027	0.0420
SST.grd	-0.0536	-0.0159	0.0219	SST.grd	-0.0443	-0.0019	0.0383
<b>Partial correlation</b>				<b>Partial correlation</b>			
Whale	0.0018	0.0623	0.1193	Krill	0.0018	0.0623	0.1193
SST	-0.0497	-0.0139	0.0217	SST	-0.0264	0.0125	0.0511
Depth	-0.0371	-0.0012	0.0320	Depth	-0.0198	0.0179	0.0563
Slope	-0.0385	-0.0019	0.0359	Slope	-0.0480	-0.0023	0.0424
SST.grd	-0.0547	-0.0166	0.0214	SST.grd	-0.0427	-0.0004	0.0389

**Table 6:** 2.5%, 50%, and 97.5% posterior quantiles of the correlation coefficients and partial correlations based on the method of Hoff (2007), BGC.

(a) Krill				(b) Whale			
	2.5%	Median	97.5%		2.5%	Median	97.5%
<b>Correlation</b>				<b>Correlation</b>			
Whale	0.0945	0.1355	0.1794	Krill	0.0945	0.1355	0.1794
SST	-0.1531	-0.1156	-0.0806	SST	-0.2047	-0.1653	-0.1263
Depth	0.0951	0.1303	0.1640	Depth	-0.0455	-0.0075	0.0315
Slope	0.0660	0.1029	0.1396	Slope	0.0656	0.1032	0.1431
SST.grd	-0.0772	-0.0406	-0.0040	SST.grd	-0.0873	-0.0497	-0.0104
<b>Partial correlation</b>				<b>Partial correlation</b>			
Whale	0.0755	0.1177	0.1617	Krill	0.0755	0.1177	0.1617
SST	-0.0913	-0.0523	-0.0162	SST	-0.1775	-0.1378	-0.0970
Depth	0.0898	0.1253	0.1591	Depth	-0.0850	-0.0453	-0.0042
Slope	0.0542	0.0888	0.1258	Slope	0.0239	0.0619	0.1018
SST.grd	-0.0590	-0.0225	0.0145	SST.grd	-0.0691	-0.0318	0.0090

## 6 Discussion

We discuss here the limitations of our method based on its application in Section 5. As the proposed method, we employ a Gaussian process with a covariance matrix that assumes isotropy and common spatial range parameter  $\phi$  across all outcomes. Although such a

simple Gaussian process facilitates efficient inference algorithms, it may struggle to fit data collected along transect lines or outcomes in which the degree of spatial correlation decay varies with distance, as illustrated by Figure 3. The assumption of isotropy implies that all locations equidistant from a given point have the same spatial correlation, which leads to identical spatial correlations between data points on the same transect line and those on different transect lines. One way to mitigate these issues is to employ Gaussian processes with more complex covariance structures, such as covariance functions that incorporate transect lines, anisotropic and nonstationary covariance functions (Paciorek and Schervish, 2006), spatiotemporal covariance functions (Cressie and Huang, 1999; Stein, 2005), and multivariate cross-covariance functions (Gneiting et al., 2010; Apanasovich et al., 2012). However, the use of such complex Gaussian processes increases the computational burden on inference algorithms, highlighting the need for more scalable algorithmic developments.

The proposed method can be applied and extended in several ways. The first is a Gaussian process formulation for the latent variables, from which we can obtain the posterior predictive distribution of the latent variables in arbitrary spatial locations (including non-sampled locations). Then, using the marginal distribution of each outcome estimated in a parametric or non-parametric manner, we can perform spatial predictions in non-sampled locations. Second, although this study focuses on the latent Gaussian process, the proposed method may be conceptually extended to other copula models, such as elliptical copulas and skew elliptical copulas (Smith, 2021). For example, if one is interested in the tail dependence of a latent process, it may be preferable to consider a  $t$ -copula model. However, posterior computation of additional parameters using such copula models may not be feasible. In this case, an MCMC sampler based on the Metropolis-Hastings algorithm or more efficient computational algorithms may need to be developed. Third, we extend our method to spatiotemporal data. Multivariate data may contain time and location information. For example, the data used in the application example were observed in the Southern Ocean over different periods. In the analysis of the dependence structure of such data, it may be necessary to consider both spatial and temporal correlations. To this end, we consider a hierarchical Bayesian spatiotemporal model based on extended rank likelihood. However, the development of posterior computation for the model is challenging, thus, a subject to address in future work. Finally, although the proposed methodology is



for point-referenced data, it is possible to develop a similar method to estimate the copula for multivariate data observed on a graph.

## Acknowledgements

This research was supported by JSPS KAKENHI (grant numbers 20H00080, 21H00699, and 24K23870).

## References

- Apanasovich, T. V., M. G. Genton, and Y. Sun (2012). A valid matérn class of cross-covariance functions for multivariate random fields with any number of components. *Journal of the American Statistical Association* 107(497), 180–193.
- Banerjee, S., B. P. Carlin, and A. E. Gelfand (2003). *Hierarchical Modeling and Analysis for Spatial Data*. Chapman and Hall/CRC.
- Biuw, M., U. Lindstrøm, J. Jackson, M. Baines, N. Kelly, G. McCallum, G. Skaret, and B. Krafft (2024). Estimated summer abundance and krill consumption of fin whales throughout the scotia sea during the 2018/2019 summer season. *Scientific Reports* 14(7493).
- Botev, Z. I. (2017). The normal law under linear restrictions: simulation and estimation via minimax tilting. *Journal of the Royal Statistical Society Series B: Statistical Methodology* 79(1), 125–148.
- Botev, Z. I. and L. Belzile (2021). Truncatednormal: Truncated multivariate normal and student distributions, r package version 2.2.2.
- Cressie, N. and H.-C. Huang (1999). Classes of nonseparable, spatio-temporal stationary covariance functions. *Journal of the American Statistical association* 94(448), 1330–1339.
- Damien, P. and S. G. Walker (2001). Sampling truncated normal, beta, and gamma densities. *Journal of Computational and Graphical Statistics* 10(2), 206–215.

- Datta, A., S. Banerjee, A. O. Finley, and A. E. Gelfand (2016). Hierarchical nearest-neighbor gaussian process models for large geostatistical datasets. *Journal of the American Statistical Association* 111(514), 800–812.
- Dey, D., A. Datta, and S. Banerjee (2022). Graphical gaussian process models for highly multivariate spatial data. *Biometrika* 109(4), 993–1014.
- Feng, C. and C. Dean (2012). Joint analysis of multivariate spatial count and zero-heavy count outcomes using common spatial factor models. *Environmetrics* 23(6), 493–508.
- Geweke, J. (1991). Efficient simulation from the multivariate normal and student-t distributions subject to linear constraints and the evaluation of constraint probabilities. In *Proceedings of 23rd Symposium on the Interface between Computing Science and Statistics*, pp. 571–578. Interface Foundation of North America: Fairfax Station, VA.
- Gneiting, T., W. Kleiber, and M. Schlather (2010). Matérn cross-covariance functions for multivariate random fields. *Journal of the American Statistical Association* 105(491), 1167–1177.
- Gong, Y. and R. Huser (2022). Flexible modeling of multivariate spatial extremes. *Spatial Statistics* 52, 100713.
- Heaton, M. J., A. Datta, A. O. Finley, R. Furrer, J. Guinness, R. Guhaniyogi, F. Gerber, R. B. Gramacy, D. Hammerling, M. Katzfuss, et al. (2019). A case study competition among methods for analyzing large spatial data. *Journal of Agricultural, Biological and Environmental Statistics* 24, 398–425.
- Heller, G. and J. Qin (2001). Pairwise rank-based likelihood for estimation and inference on the mixture proportion. *Biometrics* 57(3), 813–817.
- Hoff, P. D. (2007). Extending the rank likelihood for semiparametric copula estimation. *The Annals of Applied Statistics* 1(1), 265–283.
- Joe, H. (2014). *Dependence modeling with copulas*. CRC press.
- Jordan, M. (2004). Graphical models. *Statistical science* (1), 140–155.

- Katzfuss, M. and J. Guinness (2021). A general framework for vecchia approximations of gaussian processes. *Statistical Science* 36(1), 124–141.
- Kotecha, J. H. and P. M. Djuric (1999). Gibbs sampling approach for generation of truncated multivariate gaussian random variables. In *1999 IEEE international conference on acoustics, speech, and signal processing. Proceedings. ICASSP99 (Cat. No. 99CH36258)*, Volume 3, pp. 1757–1760. IEEE.
- Krafft, B., G. Macaulay, G. Skaret, T. Knutsen, O. Bergstad, A. Lowther, G. Huse, S. Fielding, M. E. Trathan, P. S. Choi, S. Chung, I. Han, K. Lee, X. Zhao, X. Wang, Y. Ying, X. Yu, K. Demianenko, V. Podhornyi, K. Vishnyakova, L. Pshenichnov, A. Chuklin, H. Shyshman, M. Cox, K. Reid, G. Watters, C. Reiss, J. Hinke, J. Arata, O. Godø, and Hoem (2021). Standing stock of antarctic krill (*euphasia superba* dana, 1850)(*euphausiacea*) in the southwest atlantic sector of the southern ocean, 2018-2019. *Journal of Crustacean Biology* 41(3), 1–17.
- Krock, M. L., W. Kleiber, D. Hammerling, and S. Becker (2023). Modeling massive highly-multivariate nonstationary spatial data with the basis graphical lasso. *Journal of Computational and Graphical Statistics* (just-accepted), 1–25.
- Krupskii, P. and M. G. Genton (2019). A copula model for non-gaussian multivariate spatial data. *Journal of Multivariate Analysis* 169, 264–277.
- Krupskii, P., R. Huser, and M. G. Genton (2018). Factor copula models for replicated spatial data. *Journal of the American Statistical Association* 113(521), 467–479.
- Liu, H., Y.-S. Ong, X. Shen, and J. Cai (2020). When Gaussian process meets big data: A review of scalable GPs. *IEEE transactions on neural networks and learning systems* 31(11), 4405–4423.
- Liu, J. S. and Y. N. Wu (1999). Parameter expansion for data augmentation. *Journal of the American Statistical Association* 94(448), 1264–1274.
- Manly, B. F. and J. A. N. Alberto (2016). *Multivariate statistical methods: a primer*. Chapman and Hall/CRC.

- Mann, K. H. and J. R. Lazier (2005). *Dynamics of marine ecosystems: biological-physical interactions in the oceans*. John Wiley & Sons.
- Musafer, G. N., M. H. Thompson, R. C. Wolff, and E. Kozan (2017). Nonlinear multivariate spatial modeling using nlpc and pair-copulas. *Geographical Analysis* 49(4), 409–432.
- Paciorek, C. J. and M. J. Schervish (2006). Spatial modelling using a new class of non-stationary covariance functions. *Environmetrics* 17(5), 483–506.
- Pakman, A. and L. Paninski (2014). Exact hamiltonian monte carlo for truncated multivariate gaussians. *Journal of Computational and Graphical Statistics* 23(2), 518–542.
- Pettitt, A. N. (1982). Inference for the linear model using a likelihood based on ranks. *Journal of the Royal Statistical Society: Series B (Methodological)* 44(2), 234–243.
- R Core Team (2024). *R: A Language and Environment for Statistical Computing*. Vienna, Austria: R Foundation for Statistical Computing.
- Smith, M. S. (2021). Implicit copulas: An overview. *Econometrics and Statistics*.
- Solvang, H. K., S. Imori, M. Biuw, U. Lindstrøm, and T. Haug (2024). Categorical data analysis using discretization of continuous variables to investigate associations in marine ecosystems. *Environmetrics* 35(6), e2867.
- Souris, A., A. Bhattacharya, and D. Pati (2018). The soft multivariate truncated normal distribution with applications to bayesian constrained estimation. *arXiv preprint arXiv:1807.09155*.
- Stein, M. L. (2005). Space–time covariance functions. *Journal of the American Statistical Association* 100(469), 310–321.
- Tett, P., R. Gowen, S. Painting, M. Elliott, R. Forster, D. Mills, E. Bresnan, E. Capuzzo, T. Fernandes, J. Foden, et al. (2013). Framework for understanding marine ecosystem health. *Marine Ecology Progress Series* 494, 1–27.
- Torabi, M. (2014). Spatial generalized linear mixed models with multivariate car models for areal data. *Spatial Statistics* 10, 12–26.

Vecchia, A. V. (1988). Estimation and model identification for continuous spatial processes.  
*Journal of the Royal Statistical Society Series B: Statistical Methodology* 50(2), 297–312.